JOURNAL OF AIRCRAFT
Vol. 33, No. 3, May–June 1996

Reduction of Vertical Tail Buffet Response Using Active Control

R. M. Hauch,* J. H. Jacobs,† and C. Dima‡
McDonnell Douglas Aerospace, St. Louis, Missouri 63166
and
K. Ravindra§
Parks College of St. Louis University, Cahokia, Illinois 62206

The active vertical tail (AVT) successfully reduced the buffet response of structures by utilizing piezoelectric actuators, strain gauge sensors, and simple control techniques. The AVT is a 5%-scale aeroelastically tailored structure that exhibits vibration response similar to a full-scale aircraft structure, and was designed such that it's piezoelectric actuators could provide control authority in the first two bending modes. The AVT was wind-tunnel tested on a generic twin-tailed double-delta fighter model at angles of attack and dynamic pressures representative of actual aircraft flight envelopes. At high angles of attack, the model's leading-edge vortices impinge upon the AVT. Simple control algorithms were used with piezoelectric actuators and collocated strain gauge sensors to either minimize the acceleration at the AVT's tip or the strain at the root of the tail. Control gains were verified to be a nonlinear function of angle of attack, dynamic pressure, and location of the actuator/sensor pair. Spectral analysis showed that the peak response of the controlled AVT was up to 65% lower than the uncontrolled response. This represents approximately an order of magnitude improvement in the fatigue life of a similar aircraft structure. The rms response below 200 Hz was reduced by over 20%.

Nomenclature

f = frequency, Hz
n = nondimensional frequency parameter, fx/V_∞
q = dynamic pressure, lb/ft^2
V_∞ = freestream velocity, ft/s
x = distance from wing apex, in.
α = angle of attack, deg
ε = strain, μin./in.

Introduction

MODERN fighter aircraft designs have incorporated leading-edge extensions (LEXs) and/or blending of the wing and fuselage to improve the maneuvering and performance. LEXs have been used on the F-5, F/A-18, and AV-8B, whereas some of the most well-known instances of wing/body blending include the F-16, SR-71, F-22, YF-23, MiG-29, Su-27, B-1, and B-2. Both of these types of aerodynamic configurations generate moderate-to-high-angles-of-attack stable vortex flowfields that improve the lift-to-drag ratio. Vertical tails can be placed within this high-energy flowfield to maximize rudder effectiveness, control authority, and overall aircraft directional stability at high angles of attack.[1] However, the loads induced by the resulting vortex impingement cause severe structural design requirements, which typically add unwanted structural weight.

The point at which the vortex flowfield breaks down, known as the vortex burst point, moves forward as the aircraft's angle of attack is increased. Additionally, the flowfield aft of burst is intensely random and turbulent. During some in-flight maneuvering conditions, the vortex burst point can be located upstream of the empennage structure. The turbulent flow in this burst region can then impinge upon the aft structure and cause large structural vibrations and premature structural fatigue.[2] Figure 1 shows one example of an aircraft with vortex flow enveloping the empennage structure.

Spectral analysis of the vortex flowfield both before and after burst has shown that unsteadiness within this field produces peaks in the pressure spectra, the frequency of which is related to the rotational speed of the vortex flow.[3] When this frequency is normalized with the distance from the vertex of the vortex core and with the freestream velocity, the resulting nondimensional frequency n is nearly constant and is independent of Reynolds number.[3,4] The nondimensional frequency, however, decreases with increasing angle of attack.[5,6]

At particular angles of attack and dynamic pressures, the primary vortex frequencies (i.e., the frequencies of the spectral peaks) may occur near the natural resonances of the vertical tail, horizontal tail, or other empennage substructures. When

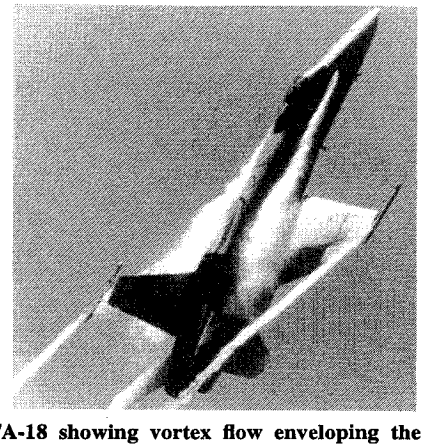

Fig. 1 F/A-18 showing vortex flow enveloping the empennage structure.

Presented as Paper 95-1080 at the AIAA/ASME/ASCE/AHS/ASC 36th Structures, Structural Dynamics, and Materials Conference, New Orleans, LA, April 10–12, 1995; received June 17, 1995; revision received Feb. 1, 1996; accepted for publication Feb. 2, 1996.

*Senior Engineer, D341, P.O. Box 516. Member AIAA.
†Deputy Team Leader, D341, P.O. Box 516. Senior Member AIAA.
‡Engineer, D341, P.O. Box 516. Member AIAA.
§Professor, Aerospace Engineering. Associate Fellow AIAA.

this occurs, the large amplitude structural oscillations cause rapid accumulation of fatigue damage, and result in premature structural failure.

There are several methods available for alleviating buffet. The position and structure of the vortex have been controlled or altered using a variety of techniques, including blowing, suction, fences, and variable position leading-edge extensions.[7-14] There have also been several attempts to reduce the buffeting on the F/A-18 using LEX deflections, dorsal-fin extensions, and a rigid fence on the upper surface of the F/A-18 LEX (Ref. 11). The latter approach successfully reduced the buffeting while the effect on aircraft pitching moment and lift was minimized.[12] It was also shown that the fences had little effect on the longitudinal position of vortex breakdown, although the vertical location and shape of the flowfield was altered.[13] However, the LEX fences reduced the unsteady pressures on the vertical tail.[12-14]

Supplementing successful aerodynamic control techniques with those reducing the structural response will provide the greatest benefit for structural fatigue life. The current potential of intelligent control systems and smart structures offers a new approach to reduce the structural response.[15] Smart materials, especially piezoelectric actuators, offer several advantages over passive stiffening, passive damping, or upstream aerodynamic devices. These advantages include, but are not limited to, multimodal response reduction, distributed actuation, and adaptive control schemes optimized for varying flight conditions.

Piezoelectric actuators mounted to the support structure of a small wind-tunnel airfoil model were used in conjunction with a simple control algorithm to successfully increase the structural damping of the airfoil while in a buffet environment.[16] This study is a pilot effort to validate the concept of actively controlling the buffet response using piezoelectric actuators in a wind-tunnel environment.

Model Description

The generic fighter model used in this experimental study was originally designed and fabricated for cooperative buffet and vortex research between McDonnell Douglas Aerospace (MDA) and NASA Langley Research Center (NASA LaRC), and can be assembled into different configurations using a combination of nose shapes and vertical tail locations. The configuration chosen for the present work was that of a 76-/40-deg double delta wing with twin vertical tails, one rigid and the other an actively controlled flexible tail (see Fig. 2). The double delta wing had an aspect ratio (based on the root chord) of 1.79, a mean aerodynamic chord of 6.7 in., and a maximum thickness of 3.3% of root chord. The fineness ratio, or the ratio of the root chord of the 76-deg nose to that of the 40-deg main wing, was 0.6. The model had a flat upper surface, sharp leading edges, and steel plates mounted between the vertical tails that prevented the flow under the wing from interacting with the tails during high-angle-of-attack conditions. A schematic of the generic fighter model is given in Fig. 3.

One of the two vertical tails mounted to the model was the active vertical tail (AVT). The AVT is an aeroelastic structure

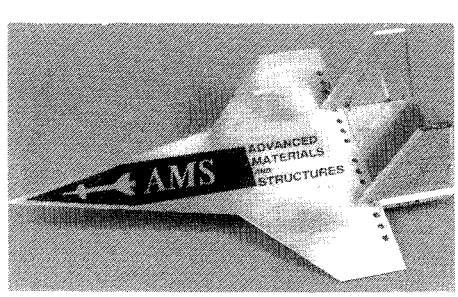

Fig. 2 Generic twin-tailed fighter model used in AVT wind-tunnel tests.

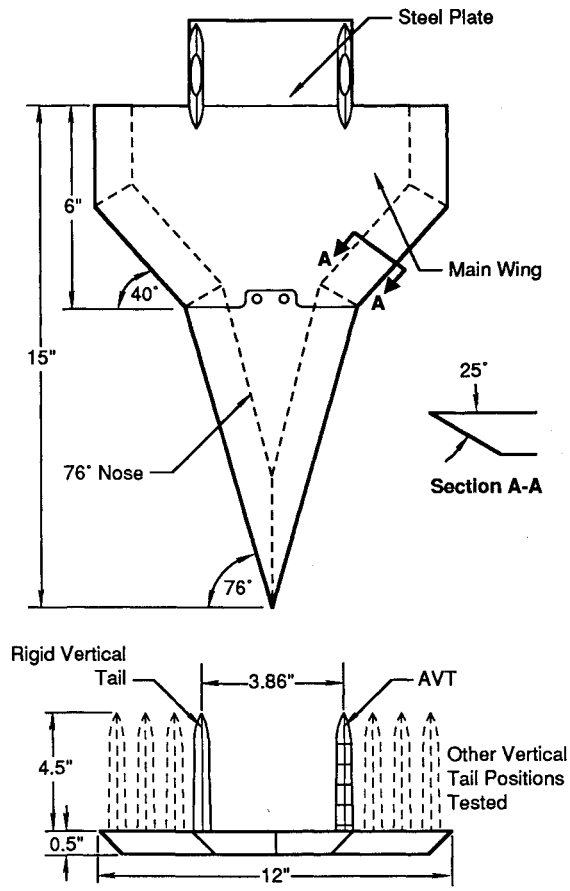

Fig. 3 Schematic of generic twin-tailed fighter model.

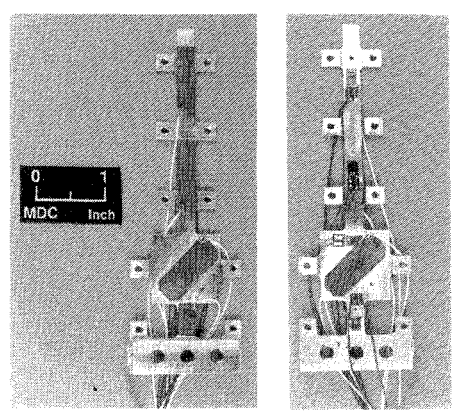

Fig. 4 AVT spar showing piezoelectric actuators and strain gauge sensors.

consisting of an aluminum spar, wood airfoil sections, piezoelectric actuators, and strain gauges (see Fig. 4). The wooden airfoil sections provided protection for the underlying components as well as aerodynamic shaping. The sections were made of maple to take advantage of that material's density, strength, and ease of fabrication. The airfoil sections were attached to the spar with small bolts, allowing them to be removed to provide access to the spar and its instrumentation.

Typically with vertical tail buffet, the structural response in the lowest modes causes the majority of damage. To control these lower bending and torsion modes, the placement of the actuators was a driving factor in the design of the AVT. Additionally, the dynamic response of the AVT was to be representative of a full-scale fighter aircraft vertical tail structure.[5] Thus, the airfoil sections were attached to the spar at discrete points to minimize the airfoil sections' contribution to the

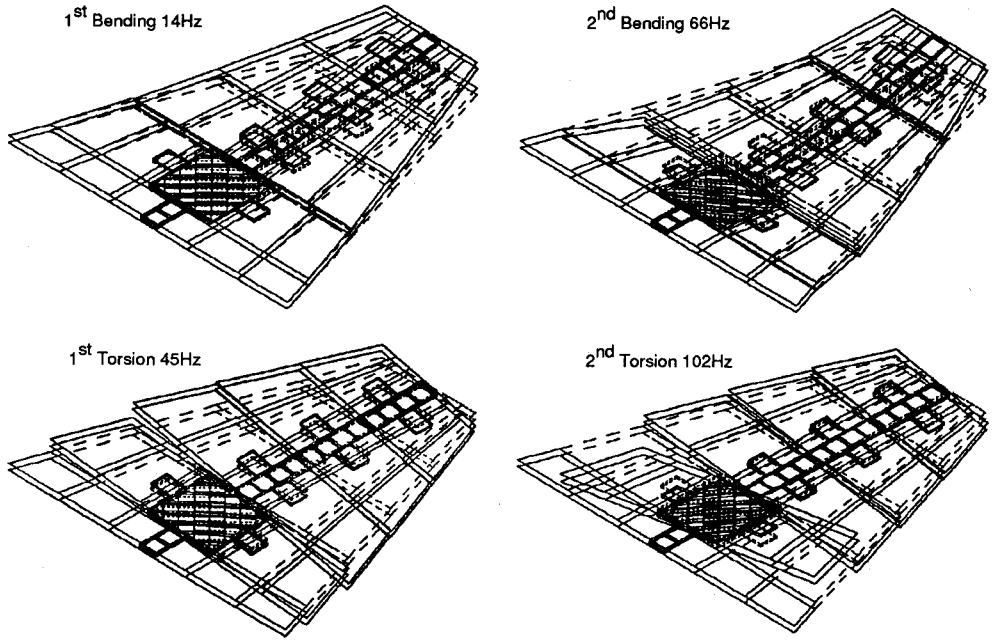

Fig. 5 Mode shapes of AVT model.

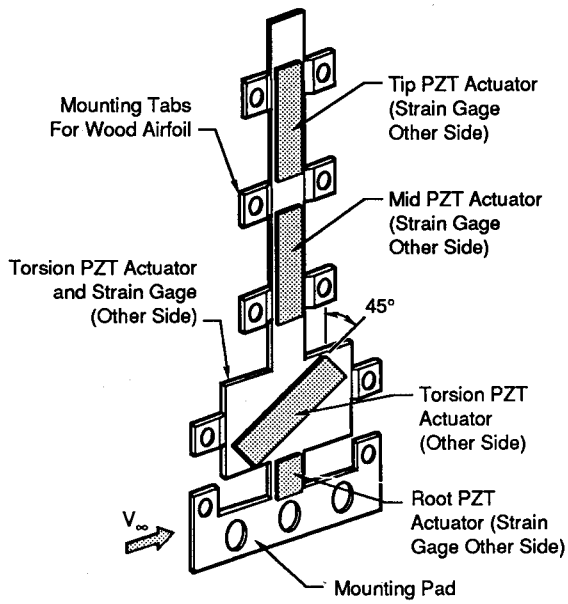

Fig. 6 Schematic of AVT spar.

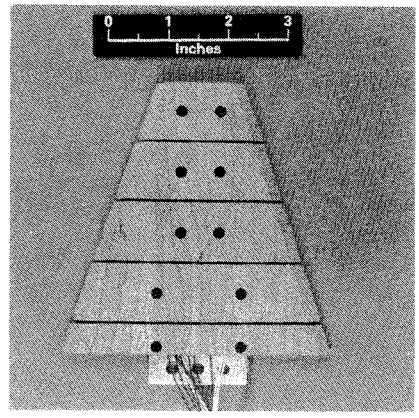

Fig. 7 Active vertical tail.

AVT's bending and torsion stiffness. This simplified the design of the spar, which also needed to have sufficient surface area for placement of the piezoelectric actuators, which were to control the lowest bending and torsion modes.

The natural frequencies and mode shapes of the spar and airfoil sections were predicted using an ABAQUS finite element model (FEM). The mode shapes and frequencies of the first four natural modes of the spar and wood airfoil sections are shown in Fig. 5. The final locations of the actuators were based upon the finite element model's mode shapes and strain energy distributions of the relevant modes. A drawing of the spar with its actuators is shown in Fig. 6, and a photograph of the assembly is given in Fig. 7. The actuators mounted along the spar length were used only for bending control, whereas the diagonally placed actuators enable control of the first torsion mode.

Although the actuators consisted of two layers of piezoelectric material (i.e., a bimorph design), the actuators were operated as a single monomorph unit. In the monomorph configuration, the actuators provided a greater bending moment since the actuators were located off of the neutral axis of the spar. The actuator material was added to the finite element model, and structural response, natural frequencies, and modes shapes of the AVT assembly were computed. Because methods for directly modeling the dynamic piezoelectric effect using the ABAQUS analysis package were not available, concentrated moments were applied at the actuator locations on the FEM.

In addition to the AVT, the generic fighter model had a rigid vertical tail to provide flow symmetry. Both the AVT and the rigid tail had similar geometric characteristics: each had an aspect ratio of 1.5, a height of 4.5 in. (0.67 of mean aerodynamic chord), and a root thickness-to-chord ratio of 0.07. The two vertical tails were positioned at various spanwise locations, ranging from 9 to 74% of the semispan, and were located such that the trailing edge of the wing was at 22% of the tails' root chord. The planform of each tail is trapezoidal and symmetric about the 50% chord line. This shape was dictated by the desire to have a vertical elastic axis so that each piezoelectric actuator could be dedicated for controlling the bending or torsion modes.

An accelerometer mounted externally at the leading edge tip of the AVT measured the lateral (spanwise) acceleration. This signal was referenced to that of another accelerometer mounted on the AVT's support boom just below the steel plate between the tails; the difference in the signals provided the acceleration

Table 1 Optimized gain settings for base and tip actuator control configuration, q = 3.0 lb/ft^2

Angle of attack	Root			Tip		
	Proportional	Integral	Differential	Proportional	Integral	Differential
10	40	0	0.25	1200	0	0
15	40	0	0.30	1200	0	0
20	40	0	0.35	1200	0	0
25	40	0	0.40	1200	0	0
30	40	0.5	0.45	1400	0.5	0.25
35	40	1.0	0.50	1600	1.0	0.50
40	50	1.0	0.55	1800	0.5	0.25
45	60	1.0	0.60	2000	1.0	1.0

of the AVT's tip relative to its base. Additionally, strain gauges were mounted to the aeroelastic tail's spar on the opposite side of each actuator. These were used to measure the bending and torsion response of the structure and to provide feedback signals to the controllers.

Test Facility and Test Conditions

The data acquisition system consisted of an eight-channel input/output data acquisition board with a digital signal processing sister board (Intelligent Instrumentation PCI-20019M-3, PCI-20021M-1B, and PCI-20201M-3) installed on a personal computer. Analog high- and low-pass filters, strain gauge signal conditioners, and accelerometer charge amplifiers were also used. AVT tip acceleration, tail support boom acceleration, four spar strains, temperature, and dynamic pressure were collected in real-time and output signals computed on the personal computer by software developed by MDA. For each angle of attack and dynamic pressure condition, over 30 s of data were collected on each channel. Each of these data sequences was then postprocessed using LabView® by computing and averaging 20 power spectral density (PSD) estimates, overlapping each PSD's time segment by 50%. Additionally, rms values of each signal were computed from the time history and from the PSD. Modal rms values for each peak were computed using a 12-Hz bandwidth. Finally, all data were checked to ensure that it was repeatable.

The experiments were conducted in the Department of Aerospace and Mechanical Engineering Low-Speed Wind Tunnel at Parks College. The open circuit tunnel has a 28 by 40 in. test section and is capable of continuous operation at velocities up to 220 ft/s, corresponding to a Reynolds number of 1.4 × 10^6/ft. The turbulence intensity in the closed-throat test section is 0.03%. For these tests, the generic fighter model was supported by a tricycle mount attached to the model's lower surface and could be cycled between −20- and 65-deg angle of attack.

Results and Discussion

Initial Wind-Tunnel Tests

The test envelope included angles of attack between 20–55 deg, dynamic pressures between 0.5–7.0 lb/ft^2, and zero sideslip. Initially, an envelope expansion test was performed to ensure that the AVT did not flutter within the maximum dynamic pressures of the test envelope. After successful completion of the envelope expansion tests, several wind-tunnel runs attempted to locate the spanwise tail position at which the levels of buffet response were the greatest while still representing a realistic aircraft configuration. Because the response of the AVT was greatest at 31% semispan, this tail position was selected for all of the remaining wind-tunnel tests.

Uncontrolled and Controlled Response

The remaining wind-tunnel investigation was divided into two distinct segments: 1) uncontrolled and 2) controlled. Because these were the first buffet tests with this double-delta model and aeroelastic tail, the baseline uncontrolled (open-loop) buffet response was measured. Power spectral densities (PSDs) and rms

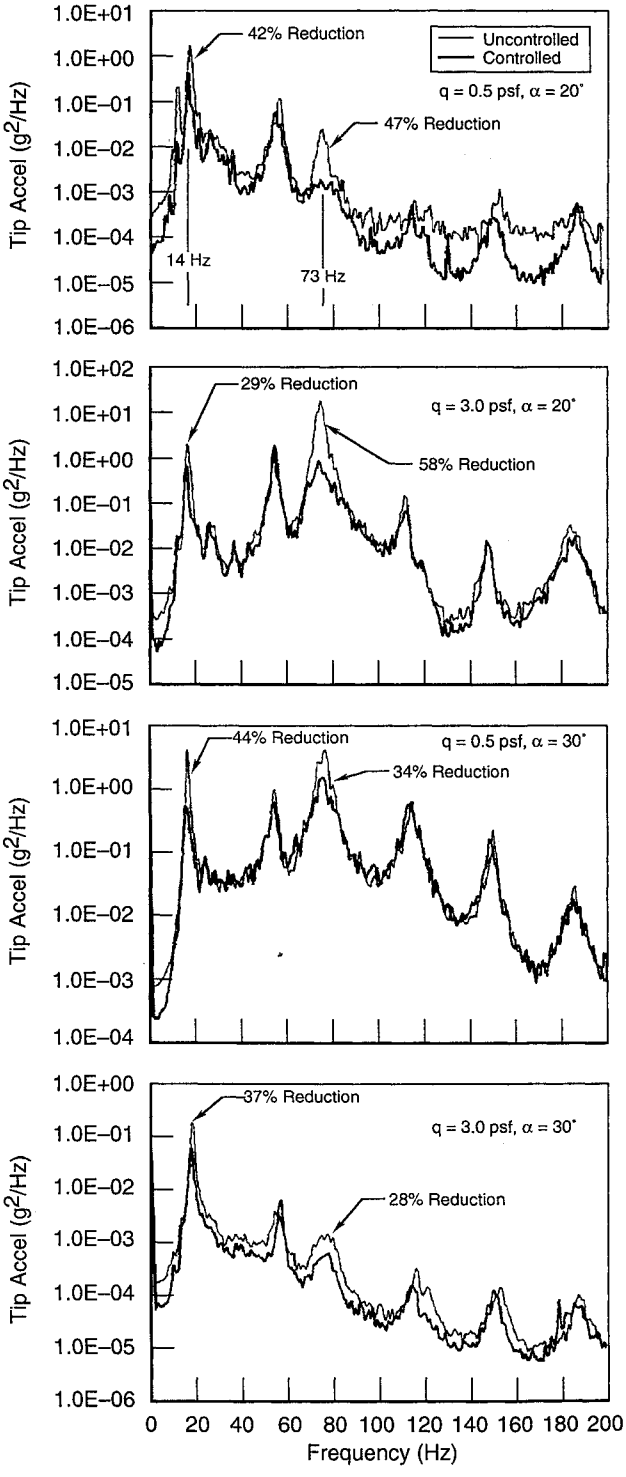

Fig. 8 Tip acceleration response PSD for uncontrolled and controlled AVT.

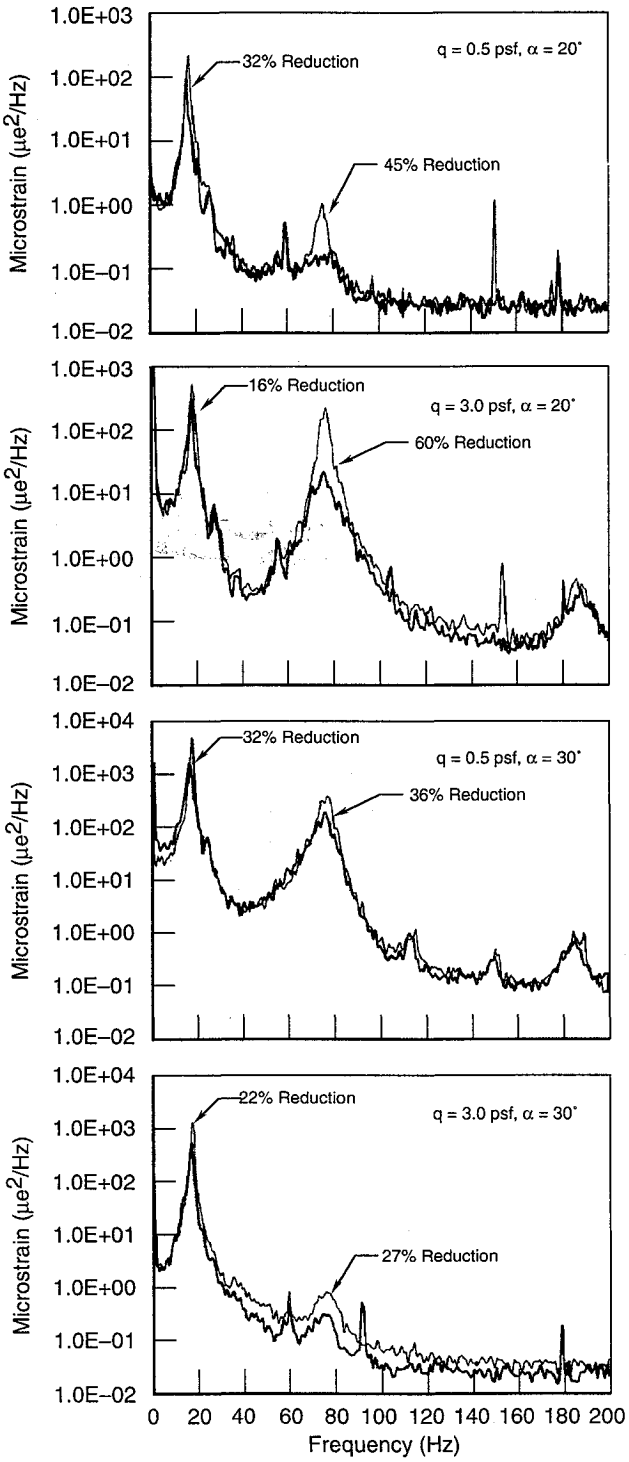

Fig. 9 Root strain response PSD for uncontrolled and controlled AVT.

values of the open-loop response were then computed at each of the test points for each of the sensor signals.

The optimum gains for the closed-loop system were determined for the same test points. At each test condition, several combinations of actuators were evaluated using proportional, integral, and differential (PID) feedback from each of the sensors. Gains that provided the minimum response of either the AVT's tip acceleration or its root strain were then used in subsequent tests. The closed-loop response of the AVT was then recorded and PSDs were computed for comparison with the open-loop results.

The optimization of the closed-loop PID settings was initiated by determining the optimum proportional gain for the root actuator/sensor pair alone to minimize either root rms strain or tip rms acceleration. Once this value was found for each dynamic pressure and angle of attack, the integral and differential gain settings were determined while leaving the proportional gain setting fixed to its optimum value. Once the root actuator/sensor pair was totally optimized for PID settings, the mid and tip actuator/sensor pairs (Fig. 6) were individually added into the control loop using the same optimization procedure. During the optimization of the closed-loop PID settings, it was observed that the piezoelectric actuator/sensor pair at the spar root contributed the majority of the response reduction authority. The other combinations using the mid and tip actuators did improve the response reduction results slightly for certain conditions over the results with only the root actuator/sensor pair. An example of the optimum closed-loop gain settings determined for a dynamic pressure of 3.0 lb/ft^2 using the root and tip actuators is given in Table 1. Similar results were obtained for the range of dynamic pressures of 0.5–5.5 lb/ft^2. It was determined that the optimum closed-loop gain settings for each actuator/sensor pair was a complex function of angle of attack, dynamic pressure, and a combination of various actuator/sensor pairs. It was beyond the scope of the present study to automate this gain scheduling procedure so that all combinations and their effects could be quantified. Hence, a reduced set of conditions and actuator combinations were focused on so as to concentrate on demonstrating the concept of active buffet response alleviation. More recent work utilizing neural networks to optimize gain settings shows promise in automating this procedure.

The uncontrolled and controlled tip acceleration responses using the single root actuator/sensor pair for four of the selected test conditions are given in Fig. 8. One result noted is that the power of the tip's acceleration response is larger for the higher angle-of-attack conditions. As can be seen in the PSDs, the first four natural modes all appear in the response. With control enabled, the peaks of the first bending mode (~14 Hz) and the second bending mode (~74 Hz) were reduced substantially; the second bending mode peak was almost eliminated in three of the four PSDs shown in Fig. 8. The rms levels of the first and second bending mode peaks (the rms level of the 12-Hz band around the natural frequency) were reduced by up to 58%, while the total rms response over the entire 200-Hz bandwidth was reduced by at least 21%. Note that while these peaks were lowered, none of the lower torsion mode peaks seem to have been favorably or adversely affected.

The uncontrolled and controlled results for the root strain PSDs are given in Fig. 9. Because of the orientation and location of the strain gauge, this sensor did not record the response of the first and second torsion modes. However, even though the signal-to-noise ratio of the strain gauges is smaller than that for the tip acceleration, the substantial reduction in the first and second bending mode response can easily be seen. Reductions in modal rms levels for these conditions range up to 60%.

Conclusions

A representative model-scale aeroelastic structure that included piezoelectric control elements was designed, analyzed, fabricated, and tested. During this investigation, reductions of up to 40% of vertical tail buffet response for varying α–q combinations was demonstrated using piezoelectric actuators. The optimal gain settings for the PID control system were verified to be complex function of angle of attack, dynamic pressure conditions, and the minimization objective. Reduction levels of rms strain during these tests indicate that a doubling of structural fatigue life could be achieved for similar full-scale aircraft empennage structures, assuming that the active elements could be scaled appropriately. In addition, this study has shown that adaptive control algorithms, which learn the appropriate control settings as function of flight condition, are

required to compensate for drastic changes in flight condition that accompany maneuvering.

The promising results from this preliminary study have led to a number of related efforts in full-scale smart structure manufacturing techniques, optimization techniques for smart material integration, and adaptive neural network control schemes. Current work at McDonnell Douglas is addressing issues such as debonding, depoling, power consumption, reliability, producibility, maintainability, and cost benefits of using smart structures.[15,17] Future work in this field of active buffet control will address flight testing and full-scale development of the active control systems.

Acknowledgments

The authors wish to acknowledge the support of L. E. Pado and P. F. Lichtenwalner for their help with the data acquisition hardware and software, F. Coffey for his assistance with the wind tunnel and associated systems at Parks College, and C. E. Hedgecock for performing the flutter analyses.

References

[1]Whitford, R., *Design for Air Combat*, Jane's Publishing Corp., Ltd., London, 1987.

[2]Ferman, M. A., Liguore, S. L., Colvin, B. J., and Smith, C. M., "Composite 'Exoskin' Doubler Extends F-15 Vertical Tail Fatigue Life," AIAA Paper 93-1341, April 1993.

[3]Roos, F. W., and Kegelman, J. T., "Recent Explorations of Leading Edge Vortex Flowfields," NASA Langley High Angle of Attack Technology Conf., Oct. 1990.

[4]Gursul, I., "Unsteady Flow Phenomenon over Delta Wings at High Angles of Attack," *AIAA Journal*, Vol. 32, No. 2, 1994, pp. 225–231.

[5]Ferman, M. A., Patel, S. R., Zimmerman, N. H., and Gerstenkorn, G., "A Unified Approach to Buffet Response of Fighter Aircraft Empennage," CP-483, AGARD, Sept. 1990.

[6]Ravindra, K., and Jacobs, J. H., "Vortex Parameter Characterization for Buffet Applications," AIAA Paper 95-0655, Jan. 1995.

[7]Gad-el-Hak, M., and Blackwelder, R. F., "Control of Discrete Vortices from a Delta Wing," AIAA-86-1915, July 1986.

[8]Bean, D. E., Greenwell, D. I., and Wood, N. J., "Vortex Control Technique for the Attenuation of Fin Buffet," *Journal of Aircraft*, Vol. 30, No. 6, 1993, pp. 847–853.

[9]Srinivas, S., Gursul, I., and Batta, G., "Active Control of Vortex Breakdown over Delta Wings," AIAA Paper 94-2215, June 1994.

[10]Syverud, E., Farokhi, S., Taghavi, R., and Neuhart, D. H., "Aerodynamic Characteristics of a Delta Wing with a Body-Hinged Leading-Edge Extension," AIAA Paper 93-3446, Aug. 1993.

[11]Washburn, A. E., Jenkins, L. N., and Ferman, M. A., "Experimental Investigation of Vortex-Fin Interaction," AIAA Paper 93-0050, Jan. 1993.

[12]Lee, B. H. K., and Brown, D., "Wind Tunnel Studies of F/A-18 Tail Buffet," AIAA Paper 90-1432, June 1990.

[13]Martin, C. A., and Thompson, D. H., "Scale Model Measurements of Fin Buffet Due to Vortex Bursting on F/A-18," CP-497, AGARD, May 1991 (Paper 12).

[14]Meyn, L. A., and James, K. D., "Full Scale Wind Tunnel Studies of F/A-18 Tail Buffet," AIAA Paper 93-3519, Aug. 1993.

[15]Jacobs, J. H., "Integrated Design and Synthesis of Smart Material Systems: An Overview of the ARPA SPICES Program," North American Smart Structures Conf., Paper 2447-19, March 1995.

[16]Heeg, J., Miller, J. M., and Dogget, R. V., Jr., "Attenuation of Empennage Buffet Response Through Active Control of Damping Using Piezoelectric Material," AIAA Structural Dynamics and Materials Damping Conf., San Francisco, CA, Feb. 1993.

[17]Hauch, R. M., "An Industrial Approach to Static and Dynamic Finite Element Modeling of Composite Structures with Embedded Actuators," North American Smart Structures Conf., Paper 2443-50, March 1995.